Archival Report

Activity-Induced Amyloid-β Oligomers Drive Compensatory Synaptic Rearrangements in Brain Circuits Controlling Memory of Presymptomatic Alzheimer's Disease Mice

Annabella Pignataro, Giovanni Meli, Roberto Pagano, Veronica Fontebasso, Roberta Battistella, Giulia Conforto, Martine Ammassari-Teule, and Silvia Middei

ABSTRACT

BACKGROUND: A consistent proportion of individuals at risk for Alzheimer's disease show intact cognition regardless of the extensive accumulation of amyloid-β (Aβ) peptide in their brain. Several pieces of evidence indicate that overactivation of brain regions negative for Aβ can compensate for the underactivation of Aβ-positive ones to preserve cognition, but the underlying synaptic changes are still unexplored.

METHODS: Using Golgi staining, we investigate how dendritic spines rearrange following contextual fear conditioning (CFC) in the hippocampus and amygdala of presymptomatic Tg2576 mice, a genetic model for Aβ accumulation. A molecular biology approach combined with intrahippocampal injection of a γ-secretase inhibitor evaluates the impact of Aβ fluctuations on spine rearrangements.

RESULTS: Encoding of CFC increases Aβ oligomerization in the hippocampus but not in the amygdala of Tg2576 mice. The presence of Aβ oligomers predicts vulnerability to network dysfunctions, as low c-Fos activation and spine maturation are detected in the hippocampus of Tg2576 mice upon recall of CFC memory. Rather, enhanced c-Fos activation and new spines are evident in the amygdala of Tg2576 mice compared with wild-type control mice. Preventing Aβ increase in the hippocampus of Tg2576 mice restores CFC-associated spine changes to wild-type levels in both the hippocampus and amygdala.

CONCLUSIONS: Our study provides the first evidence of neural compensation consisting of enhanced synaptic activity in brain regions spared by Aβ load. Furthermore, it unravels an activity-mediated feedback loop through which neuronal activation during CFC encoding favors Aβ oligomerization in the hippocampus and prevents synaptic rearrangements in this region.

Keywords: Aβ oligomers, Alzheimer disease, Amygdala, Contextual fear conditioning, Hippocampus, Neural compensation

https://doi.org/10.1016/j.biopsych.2018.10.018

The accumulation of amyloid-β (Aβ) into plaques is one of the main hallmarks of Alzheimer's disease (AD). Although plaques are only visible in the brains of symptomatic patients, positron emission tomography (PET) scans for detection of amyloid in preplaque stages reveal that gradual amyloid accumulation starts 10 to 20 years before the occurrence of dementia symptoms in at least one third of individuals at risk for AD (1–7). Longitudinal studies confirm that the majority of those cases develop AD, but the pathophysiological events associated with Aβ accumulation during the preclinical AD stages remain largely unexplored.

As Aβ exerts a toxic effect on neurons, a question emerging from preclinical PET studies is how cognition remains intact in the presence of an amyloid load in the brain. Combined PET and functional magnetic resonance imaging studies suggest that Aβ-positive individuals can preserve intellectual abilities either by increasing the activation of Aβ-positive regions to compensate for their loss of efficiency (8,9) or by activating other regions that are not affected by the Aβ load (8,10,11). For instance, overactivation of the hippocampus, a brain region involved in memory and particularly vulnerable to Aβ deposition, was detected in young carriers of the apolipoprotein E ε4 allele (9) and in presymptomatic carriers of the *PSEN1* mutation (12), as compared with age-matched control subjects, during encoding and recall of episodic memory tasks. Also, strong activation in the cerebellum, a region not prone to Aβ accumulation, was reported in individuals at risk for AD during correct execution of a verbal encoding task (13). These findings indicate that neuronal networks rearrange to face cognitive demand; however, the understanding of synaptic changes underlying network activation or deactivation is incomplete.

The investigation of in vivo synaptic activity in human AD brains has been limited by the lack of available imaging

techniques with subcellular resolution. Nonetheless, studies that examined synaptic function in AD mouse models have shown that dysfunction of synapses parallels neuronal networks destabilization (14). Because most AD models are well characterized in terms of age-related AD progression, they represent a valid tool to investigate synaptic changes underlying Aβ-mediated network dysfunctions during preclinical AD stages.

Memory relies on the formation and strengthening of new synaptic connections within key brain regions. We extensively studied this phenomenon in rodents (15–17) using the contextual fear conditioning (CFC) paradigm. This memory task is associated with enhanced neuronal activity in the hippocampus and the amygdala, which encode for the spatial and emotional components of the task, respectively (18,19). We have reported that in mice exposed to CFC new spines grow along dendrites of neurons located in the hippocampal CA1 subregion and the basolateral amygdala (BLA) within 24 to 48 hours after CFC encoding (15–17). Synapses that are formed on these new spines sustain the persistence of memory trace (20). However, in early AD stages, the toxic effect of Aβ can affect synapse formation in the hippocampus, as this region is particularly vulnerable to Aβ accumulation (14,21). Specifically, the presence of soluble Aβ oligomers, which include several Aβ species before their accumulation into plaques, causes loss of hippocampal synapses and damages synaptic plasticity in this region (22,23); furthermore, administration of Aβ species blocks the growth of new synapses (24).

Neuronal activity increases Aβ deposition in the hippocampus (21,25,26), but no studies so far have investigated whether activity-induced endogenous Aβ alters synaptic circuits at preclinical stages of AD progression.

We formulated the hypothesis that during presymptomatic AD stages, neuronal activity associated with CFC causes Aβ rises that negatively impact CFC-induced synapse formation in this region. We hereby investigated this hypothesis in Tg2576 mice, a transgenic AD model expressing elevated Aβ (27). The aim of this study was twofold: 1) to examine whether at presymptomatic AD stages, endogenous Aβ impacts the formation of new synapses in the hippocampus, or if compensatory rearrangements take place in the alternative synaptic circuit involving the BLA, and 2) to investigate if these effects are reversible by preventing Aβ accumulation in the hippocampus.

METHODS AND MATERIALS

Transgenic Mice and Ethics Statement

Tg2576 mice heterozygous for the K670N/M671L mutation (HuAPP695swe; Taconic Biosciences, Rensselaer, NY) in a C57BL/6/SJL genetic background and wild-type (WT) littermates were used at 2 months of age. Unless otherwise indicated, male mice were used for the experiments. Animal procedures conformed with European Union directive 2010/63/EU for animal experiments and were approved by the Italian Ministry for Health.

Contextual Fear Conditioning

Mice were trained in CFC as previously described (28). Briefly, on day 1 mice received five nonsignaled foot shocks (0.7 mA,

2-second duration, separated by 58-second intervals) in a conditioning chamber (CFC encoding). On day 2 mice were re-exposed to the conditioning chamber for 5 minutes with no foot shock being delivered (CFC recall), and fear behavior (freezing) was measured. Mice were sacrificed at different time points from encoding or recall.

Immunofluorescence and Confocal Microscopy

Immunofluorescent detection of neuronal activity marker c-Fos, Aβ species (D54D2), prefibrillar oligomers (OC), C-terminal Aβ$_{42}$ (12F4), and postsynaptic marker postsynaptic density protein 95 (PSD95) was performed on brain slices containing hippocampus and amygdala by standard procedures. Images were acquired by confocal laser scanning microscopy (Zeiss LSM 700; Carl Zeiss AG, Feldbach, Switzerland) and analyzed using Imaris 7.6.5 image analysis software (Bitplane, Belfast, United Kingdom).

Dendritic Spine Analysis

Golgi-Cox staining was performed as previously described (28). Dendritic spines were analyzed on randomly selected 30-μm dendritic segments of the BLA and apical CA1 dendrites using a computer-based neuron tracing system (Neurolucida; MBF Bioscience, Williston, VT).

Protein Extraction and Immunoblotting

Hippocampal and amygdala samples were sequentially extracted in Tris-buffered saline (TBS-soluble) and TBS with 1% Triton X-100 and used for dot blot and Western blot experiments. Dot blot analyses were performed as in Meli et al. (29) with antibodies directed against Aβ$_{42}$ (295F2) or fibrillar oligomers (OC and A11). For the Western blot, antibodies directed against Aβ (D54D2), Aβ$_{42}$ (295F2), or anti-amyloid precursor protein (APP) C-terminal (A8717) were used. Densitometric analyses were performed using ImageJ software bundled with 64-bit Java 1.8.0_122 (National Institutes of Health, Bethesda, MD).

Intrahippocampal Injections

Anesthetized mice were fixed on a stereotaxic apparatus for bilateral injection of 1 μL of DAPT (3.5 mM), or vehicle (phosphate-buffered saline [PBS] 0.1M). For lidocaine injections, mice were preimplanted with guide cannulae through which injection cannulae were inserted for bilateral delivery of 1 μL lidocaine hydrochloride solution (1%) or PBS vehicle.

Data Analysis and Statistics

Experimenters blinded to the different conditions performed data analyses. Unless otherwise indicated, two-way analyses of variance with genotype/condition as between-subjects factors were used to compare group differences. One-way analysis of variance was used for differences between means. Fisher's least significant difference post hoc test was used where necessary. Differences with $p < .05$ were considered significant.

Experimental details are provided in the Supplemental Methods.

Compensatory Synaptic Changes in Preclinical AD

RESULTS

In Presymptomatic Tg2576 Mice, Recall of CFC Memory Is Associated With Overactivation of the BLA

To test patterns of neuronal activation in presymptomatic Tg2576 mice, we measured the expression of the neuronal activity marker c-Fos upon exposition to CFC (Figure 1A). Two-month-old mice were used because at that age Tg2576 mice still have intact memory (28). Indeed, we reported the same amount of freezing between Tg2576 and WT mice during CFC recall ($p > .05$) (Figure 1B).

The amygdala and hippocampus, two brain regions with a key role in memory, have been reported to activate upon CFC encoding and reactivate during CFC recall (9). To investigate if these two regions are recruited in Tg2576 mice, we measured the expression of c-Fos following both CFC encoding and recall. Based on our previous studies (16,17), we focused on the CA1 subregion of the hippocampus and the BLA.

In the subgroup of mice sacrificed after encoding, we found a general increase in the expression of c-Fos as compared with home cage (HC) control mice in both the CA1 subregion and BLA ($p < .001$ for both regions) (Figure 1C, D). No differences in c-Fos activation were found between Tg2576 and WT mice in these two regions ($p > .05$ for both regions).

However, in the subgroup of mice sacrificed after recall (Figure 1C, E), we reported CFC-induced c-Fos activation in the CA1 subregion of WT mice ($p < .01$) but not Tg2576 mice ($p > .05$). In the BLA, we detected enhanced c-Fos upon CFC recall in mice from both genotypes ($p < .01$ for WT mice and $p < .001$ for Tg2576 mice). Strikingly, this increase was more pronounced in Tg2576 mice than in their WT counterparts ($p < .05$). A plausible explanation for this effect is that hypersynchronous activity reported in the hippocampus of Tg2576 mice at this age (30) favors the overactivation of the BLA. To test this possibility, we temporally silenced the CA1 subregion of Tg2576 mice by local injection of the activity suppressor lidocaine during CFC encoding, and then measured c-Fos expression in the BLA during CFC recall (Supplemental Figure S1). We found that the CFC-induced peak of c-Fos expression in the BLA was smaller in lidocaine-injected control mice as compared with vehicle-injected control mice ($p < .05$), thereby demonstrating that the activity of the CA1 subregion modulates the activity of the BLA and suggesting the existence of homeostatic balancing between these two regions.

We then probed whether other brain regions are involved in compensatory mechanisms during CFC recall in Tg2576 mice. To do this, we selected a set of cortical and subcortical regions that are interconnected with the CA1 subregion (31). We found that c-Fos activation was comparable between WT and Tg2576 mice (Supplemental Figure S2) in almost all selected regions, with the only exception being the subiculum (the output structure of the hippocampus), in which we found a pattern of activity resembling the one in the CA1 subregion.

Together, these data indicate that although in Tg2576 mice both the hippocampus and the amygdala are recruited during the formation of a CFC memory, its recall is associated with overactivation of amygdala only, and that such overactivation

likely compensates for altered hippocampal activation to maintain intact memory performance.

Formation of Dendritic Spines in the BLA but Not in the CA1 Subregion Following CFC in Tg2576 Mice

To investigate synaptic rearrangements that underlie memory in Tg2576 mice, we tracked changes of dendritic spines in the hippocampus and the amygdala of mice exposed to CFC (Figure 2A, B). Dendritic spines were classified according to their growing level of maturity into filopodia, chubby, thin, and mushroom spines (32,33), and densities for the four spine categories were measured in Tg2576 and WT mice 24 hours after CFC recall. Although in the HC condition the density of dendritic spines was comparable between Tg2576 and WT mice, in both the CA1 subregion and BLA significant differences were reported between the two genotypes upon CFC.

In the CA1 subregion (Figure 2C), CFC recall was associated with a significant increase of mushroom spines in WT mice ($p < .001$ compared with HC control mice) but not in Tg2576 mice ($p > .05$ compared with HC control mice and $p < .01$ compared with WT mice). Also, a small nonsignificant increase of thin spines was found upon CFC recall in WT mice only ($p = .06$). These data indicate that CFC is associated with the formation of mature spines in the CA1 subregion of WT mice but not Tg2576 mice.

In the BLA (Figure 2D), a significant CFC-induced increase of thin spines was evident in Tg2576 mice ($p < .001$ compared with HC control mice) but not in WT mice ($p > .05$ compared with HC control mice and $p < .01$ compared with Tg2576 mice). Rather, a CFC-induced increase of mushroom spines was evident in both genotypes ($p < .05$ for both). Together, the above data indicate that in AD mice, spine rearrangement associated with CFC memory occurs in the BLA, mainly through the formation of new thin spines.

To probe whether thin and mushroom spines associate with synapses, we tagged brain slices with postsynaptic density protein 95, a key protein located in postsynaptic compartments of spines (34). A significant CFC-induced increase of postsynaptic density protein 95 spots was found in the CA1 subregion of WT mice and in the BLA of both WT and Tg2576 mice (Supplemental Figure S4), thereby suggesting that both thin and mushroom spines likely support active synapses.

Together, the above data indicate that synaptic rearrangements associated with CFC memory take place in the amygdala, but not in the hippocampus, of AD mice.

Exposition to CFC Encoding Is Associated With a Rise of Aβ Levels in the Hippocampus of Tg2576 Mice

The above data suggest that exposure to CFC causes alterations otherwise not evident in the hippocampus of Tg2576 mice in HC condition. To investigate whether Aβ changes upon CFC, we measured patterns of Aβ in the two regions within 24 hours from CFC encoding (Figure 3A); this time point was selected as we know that Aβ is released 30 to 60 minutes from neuronal activation (21,26).

First, we measured the overall levels of $A\beta_{42}$ in TBS extracts by a native dot blot analysis. A selective increase ($p < .05$) of
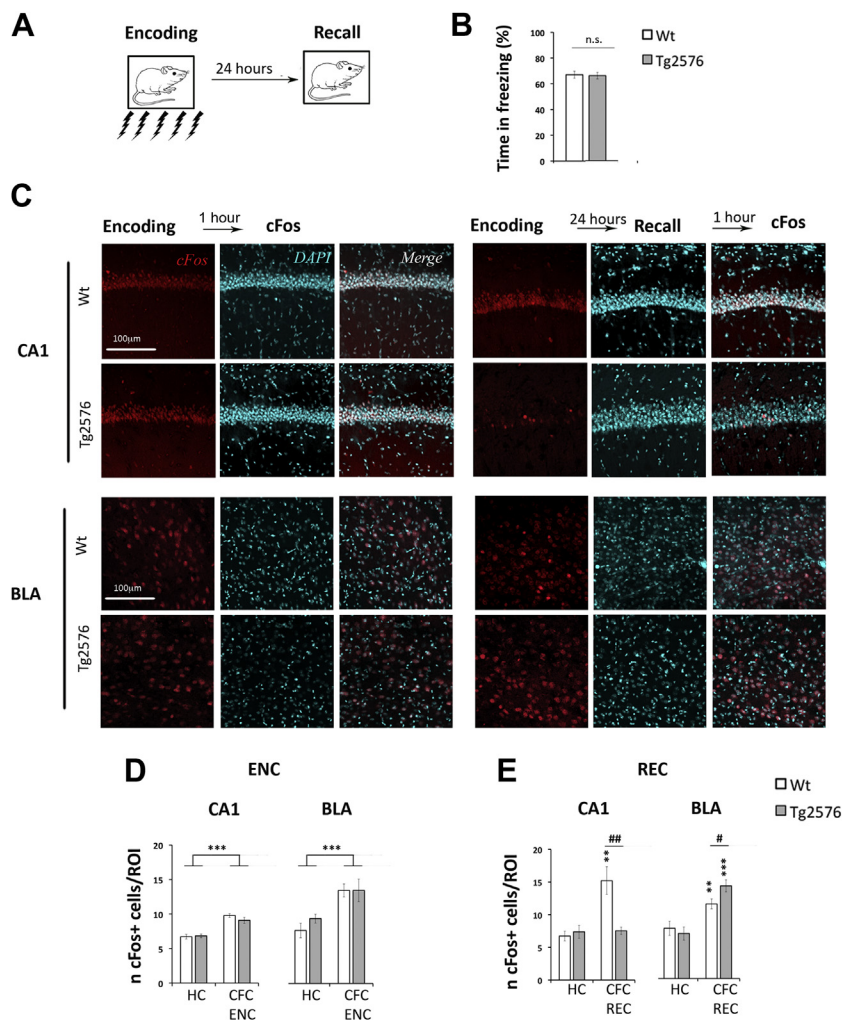
Figure 1. Different patterns of neuronal activation in Tg2576 and wild-type (Wt) mice following memory encoding and recall. **(A)** Tg2576 and Wt mice were subjected to contextual fear conditioning (CFC) consisting of exposing mice to context-shock association (encoding phase [ENC]) and re-exposing them to the context 24 hours later without delivery of the foot-shock (recall test [REC]). Two groups of mice were sacrificed for immunofluorescence either 1 hour after encoding or 1 hour after recall. Home cage (HC) control mice were sacrificed in parallel. **(B)** Fear behavior (freezing) during CFC REC is used as an index for associative memory. Freezing response was comparable between Wt and Tg2576 mice ($F_{1,13} = 0.654$, $p > .05$). Data are plotted as mean percentage time in freezing $\pm$ SEM; $n = 8$ Wt mice, 7 Tg2576 mice. **(C)** Coronal slices of the hippocampal CA1 subregion and basolateral amygdala (BLA) stained with anti–c-Fos antibody (red) and DAPI (blue). Images refer to brains from Wt and Tg2576 mice sacrificed after CFC ENC (left) and REC (right). Images of c-Fos–stained slices from Tg2576 and Wt mice in the HC control condition are shown in Supplemental Figure S1. Images were captured at 20× magnification. **(D, E)** Number of c-Fos positive spots/area (region of interest [ROI]) upon CFC ENC and REC in the CA1 subregion and BLA of Wt and Tg2576 mice. **(D)** Exposure to context-shock association increases c-Fos expression in both the CA1 subregion and the BLA, as a condition effect was evident upon CFC ENC (for the CA1 subregion [$F_{1,38} = 62.27$, $p < .001$] and for the BLA [$F_{1,32} = 24.24$, $p < .001$]); no differences in c-Fos expression were reported between the two genotypes (genotype effect: for the CA1 subregion [$F_{1,38} = 0.7$, $p > .05$] and for the BLA [$F_{1,32} = 5.1$, $p > .05$]). ***$p < .001$ compared with HC control mice. **(E)** After recall, condition effect (*) was still evident indicating increased c-Fos levels as compared with HC. In CA1, a two-way analysis of variance (genotype × condition interaction [$F_{1,39} = 8.29$, $p < .01$]) and post hoc pair comparisons revealed that increased c-Fos expression upon CFC is only evident in Wt mice. In the BLA, Tg2576 mice display increased activation as compared with both Wt mice ($F_{1,28} = 5.001$, $p < .05$) and relative HC control mice ($F_{1,21} = 21.57$, $p < .001$). Data are averaged per group and plotted as mean $\pm$ SEM; $n = 3/5$ slices per animal, 3 mice per group. **$p < .01$ and ***$p < .001$ compared with HC control mice, #$p < .05$ and ##$p < .01$ for genotype comparisons.

Aβ_{42} was detected in the hippocampus but not in the amygdala of Tg2576 mice upon CFC as compared with HC control mice (Figure 3A, B).

A further Western blot analysis showed similar changes of an Aβ immunoreactive 14-kDa band, confirmed by two independent antibodies raised against different epitopes, namely the N terminal–specific antibody D54D2 (Figure 3C, D) ($p < .01$) and the C terminal–specific anti-Aβ_{42} antibody (clone 295F2), which selectively detects Aβ_{42} but not other Aβ/APP-truncated forms (Supplemental Figure S5A). On this basis, the 14-kDa band is representative of a pool of sodium dodecyl sulfate–stable Aβ_{42}-soluble oligomers. Further details on the Aβ composition of these oligomeric species are discussed in the next section.

In line with these immunoblot results, immunofluorescent detection of Aβ by D54D2 on brain slices (Figure 3E, F) showed that Aβ signal was enhanced in the CA1 subregion but not in the BLA of Tg2576 mice after CFC encoding. Of note, Aβ signal was barely detectable in the CA1 subregion and BLA of Wt mice, but no Aβ rises were associated with CFC in this genotype (Supplemental Figure S6). The CFC-induced increase of Aβ immunostaining in the CA1 subregion was confirmed by the C terminal–specific anti-Aβ antibody 12F4 (Supplemental Figure S5B).

Together, the above results demonstrate that Aβ species were increased in the hippocampus but not in the amygdala of Tg2576 mice 24 hours after CFC encoding. Of note, Aβ_{42} species in the hippocampus were back to HC control levels 48 hours after CFC encoding (Supplemental Figure S7), thereby indicating the transitory nature of these changes.

Next, we used Morris water maze (MWM), a task with a reduced stressful component as compared with CFC, to control the impact of the stressful component of the behavioral task on the Aβ increase. In mice subjected to MWM, we found a significant increase ($p < .05$) of Aβ_{42} (Supplemental Figure S8), although this was smaller than the one found in
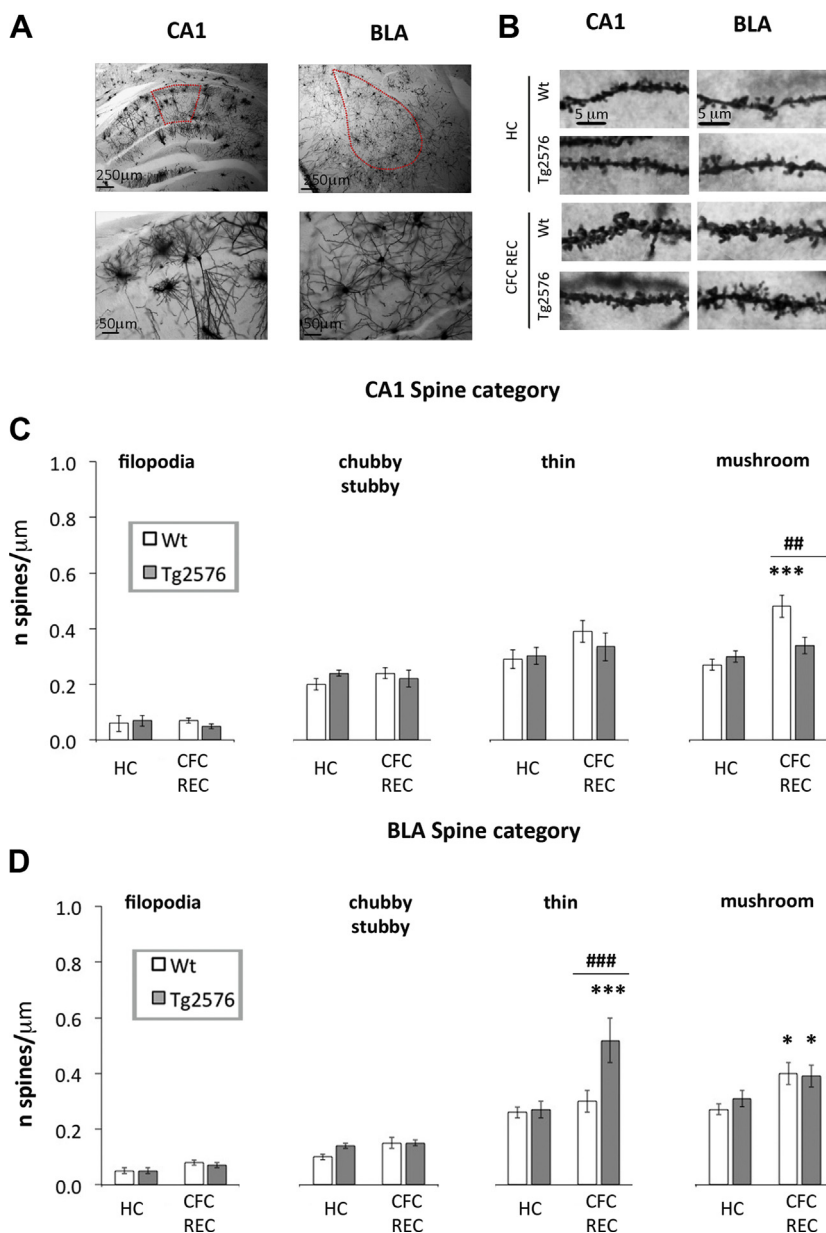
Compensatory Synaptic Changes in Preclinical AD

Figure 2. Contextual fear conditioning (CFC) recall is associated with an increase of dendritic spine number in the basolateral amygdala (BLA) of Tg2576 mice. Tg2576 and wild-type (Wt) mice were exposed to CFC encoding and recall (REC) 24 hours later. Mice were sacrificed for spine analysis 24 hours after CFC REC. Home cage (HC) control mice were sacrificed in parallel. **(A)** Representative images of Golgi staining in the hippocampal CA1 subregion and BLA acquired at 5× magnification. Areas outlined in red dots indicate regions selected for spines counting. Lower panels show examples of Golgi-stained neurons in the regions of interest (images acquired at 20× magnification). **(B)** Merge of overlapping z-stack projections captured at 100× magnification for the CA1 subregion and BLA dendritic segments. Images are representative for Wt and Tg2576 mice sacrificed after CFC REC and HC control mice. **(C)** Spine density (n spines/μm) in apical CA1 dendrites. Spines are subdivided into four distinct spine categories. Two-way analysis of variance with spine categories as repeated measures (genotype × condition interaction [$F_{1,30} = 6.61$, $p < .05$]) and post hoc pair comparisons indicate that more mushroom spines were evident in Wt mice after CFC as compared with both HC control mice and Tg2576 mice. Also, a small nonsignificant increase in the number of thin spines was evident in Wt but not Tg2576 mice after CFC as compared with relative HC control mice ($p = .06$). No differences were reported among groups for the density of filopodia ($p > .05$) and chubby/stubby spines ($p > .05$). $n = 3$ neurons per mouse, 3 mice per group. ***$p < .001$ (HC control mice); ##$p < .01$ (Tg2576 mice). **(D)** Spine density subdivided into the four spine categories in BLA neurons. Two-way analysis of variance with spine categories as repeated measures (genotype × condition interaction [$F_{1,38} = 4.39$, $p < .05$]) and post hoc pair comparisons indicate that more thin spines were evident in Tg2576 mice from the CFC REC group as compared with both relative HC control mice and Wt mice from the CFC REC group. The density of mushroom spines was significantly increased from the HC control condition in CFC-trained mice from both genotypes. No differences were reported for filopodia ($p > .05$) and chubby/stubby spines ($p > .05$). $n = 3/4$ neurons per mouse, 3 mice per group. *$p < .05$; ***$p < .001$ (HC control mice); ###$p < .001$ (Wt mice). See also Supplemental Figure S3 for total spine density values and pseudo-CFC control encoding.

mice subjected to CFC; this suggests that the amount of Aβ is proportional to the stress associated with the behavioral task.

Characterization of Aβ Species and Assembly States

To confirm the specific effect of CFC on Aβ modulation, we investigated the processing of APP and the effect of the γ-secretase inhibitor DAPT. As for APP, we reported that levels of APP-full length were unvaried in samples from the CFC encoding group. Rather, in this group we detected a trend of reduction from HC levels of β–C-terminal fragments (measured

on TBS with 1% Triton X-100 extracts representative of the membranous fraction), which is complementary to the increase of Aβ measured in TBS-Soluble extracts (Supplemental Figure S5C). Together, these data indicate that the CFC-induced effect is selective for Aβ production upon APP processing without affecting APP expression.

We then injected the γ-secretase inhibitor DAPT into the hippocampus of Tg2576 mice 15 hours before the CFC encoding trial. As expected, levels of Aβ42 in TBS extracts (Figure 4A, B; Supplemental Figure S5A) were massively reduced in DAPT-injected mice as compared with PBS-injected mice ($p < .001$). Furthermore, 14-kDa Aβ oligomers were significantly reduced in DAPT-injected mice as compared
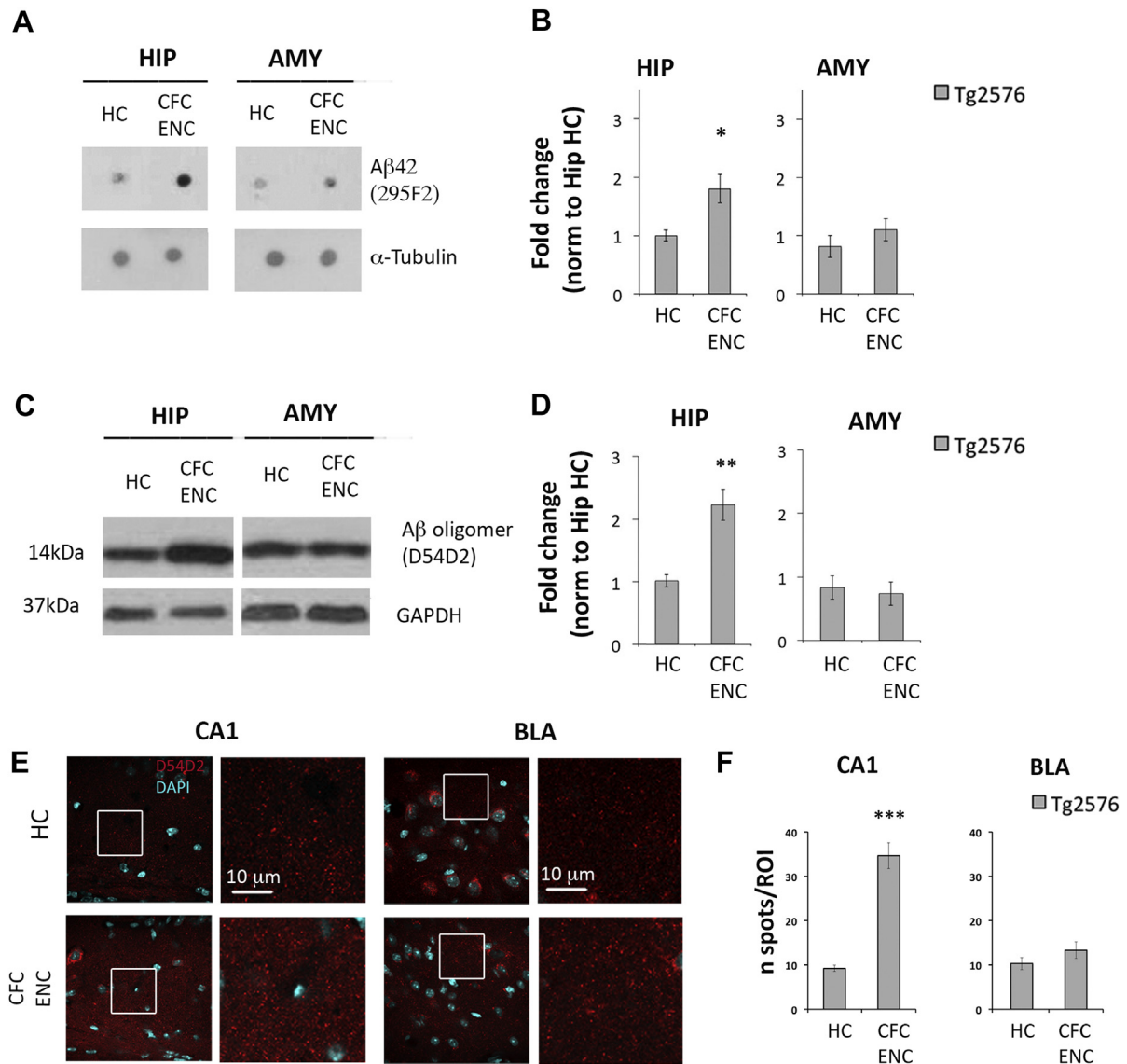
Figure 3. Contextual fear conditioning (CFC) encoding (ENC) is sufficient to increase amyloid-β (Aβ) levels in the hippocampus of Tg2576 mice. Tg2576 mice were subjected to CFC ENC and sacrificed 24 hours later for Aβ quantification by immunoblot and immunofluorescence. Home cage (HC) control mice were sacrificed in parallel. **(A)** Native dot blot analysis of Tris-buffered saline–soluble hippocampus (HIP) and amygdala (AMY) extracts from Tg2576 mice in the CFC ENC or HC groups by anti-Aβ$_{42}$ antibody (clone 295F2). α-Tubulin was used as loading control. **(B)** Quantification of Aβ$_{42}$ immunoreactivity from groups in panel **(A)**. Levels of Aβ$_{42}$ immunoreactivity were significantly increased after CFC ENC in the HIP ($F_{1,10} = 5.02$, $p < .05$) but not in the AMY ($F_{1,4} = 1.11$, $p > .05$). All data are normalized to HC hippocampal samples, averaged per group and plotted as mean ± SEM; $n = 5/7$ mice per group for HIP, 3 mice per group for AMY. **(C)** Western blot analysis of Tris-buffered saline–soluble HIP and AMY extracts from Tg2576 mice in the CFC ENC or HC groups. Anti-Aβ D54D2 detects a 14-kDa band of sodium dodecyl sulfate–stable Aβ oligomers. Glyceraldehyde 3-phosphate dehydrogenase (GAPDH) used as loading control. See Supplemental Figure S5D for further controls. **(D)** Quantitative analysis of the Aβ/GAPDH ratio from groups in panel **(C)**. Levels of 14-kDa Aβ oligomers were increased from HC levels in the HIP but not in the AMY of Tg2576 mice from the CFC ENC group (condition × region interaction [$F_{1,10} = 9.53$, $p < .05$]). All data are normalized to HC hippocampal samples, averaged per group and plotted as mean ± SEM; $n = 3/4$ mice per group. **$p < .01$ compared with HC control mice. **(E)** Aβ labeling using D54D2 antibody in coronal slices containing the hippocampal CA1 subregion and basolateral amygdala (BLA) from Tg2576 mice under the HC condition or sacrificed after CFC ENC. DAPI (blue) counterstains cell bodies. For each region, the right panels correspond to magnification of squares reported in the left panels. **(F)** Quantification of the Aβ-positive signal from brain slices in panel **(E)**. Aβ labeling was increased in the CA1 subregion ($F_{1,27} = 97.39$, $p < .001$) but not in the BLA ($F_{1,20} = 1.82$, $p > .05$) of Tg2576 mice from the CFC ENC group as compared with the HC control mice. Data are averaged per group and plotted as mean ± SEM; $n = 3/5$ slices per mouse, 3 mice per group. ***$p < .001$ compared with HC control mice.

with PBS-injected mice ($p < .001$) and were comparable to the levels of HC untreated control mice ($p > .05$) (Figure 4C, D; Supplemental Figure S5D).

To better characterize different conformations of Aβ oligomeric species, we measured fibrillar oligomers with the OC antibody (35) and prefibrillar oligomers with the A11 antibody (36)
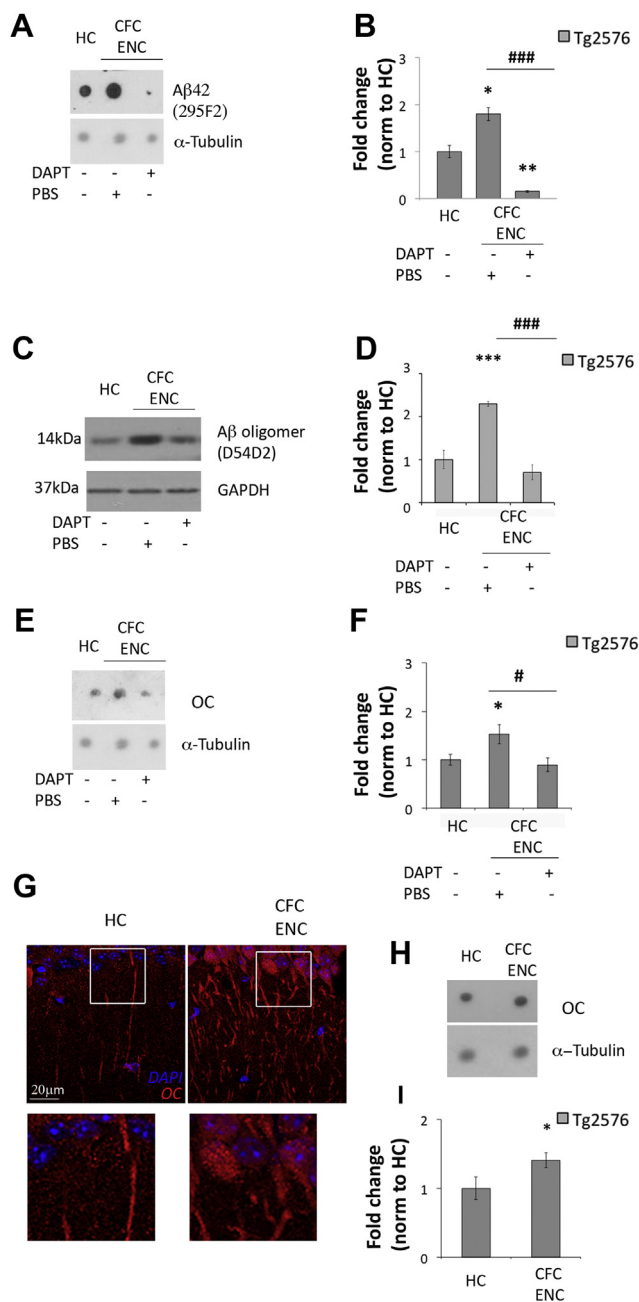
Figure 4. Amyloid-β (Aβ) species and assembly states. Mice were subjected to intrahippocampal injection of DAPT or phosphate-buffered saline (PBS) vehicle; 15 hours later they were subjected to contextual fear conditioning encoding (CFC ENC) and sacrificed after a further 24 hours for Aβ quantification by immunoblot and immunofluorescence. Home cage (HC) control mice were sacrificed in parallel. **(A)** Native dot blot analysis by anti-Aβ$_{42}$ antibody (clone 295F2) of Tris-buffered saline (TBS)–soluble hippocampus (HIP) extracts of Tg2576 mice in the CFC ENC group after DAPT/PBS injection or the HC condition. α-Tubulin was used as loading control. **(B)** Quantification of Aβ$_{42}$/α-tubulin ratio from groups in panel **(A)**. Aβ$_{42}$ levels were increased in the group of mice receiving PBS injection and decreased in the group of DAPT-injected mice as compared with the HC control mice (condition effect [$F_{2,9} = 25.96, p < .001$]). Post hoc comparison indicated a significant reduction of Aβ$_{42}$ levels in DAPT-injected mice as compared with the PBS-injected group. Data are averaged per group and

plotted as mean ± SEM; $n = 3/5$ mice per group. $*p < .05$ and $**p < .01$ compared with HC; $###p < .001$ for differences between PBS- and DAPT-injected groups. **(C)** Western blot analysis of 14-kDa Aβ oligomers from TBS-soluble HIP extracts from Tg2576 mice in the CFC ENC condition subjected to DAPT or PBS vehicle injection, or the HC control mice. Glyceraldehyde 3-phosphate dehydrogenase (GAPDH) was used as loading control. **(D)** Quantitative analysis of Aβ/GAPDH ratio from groups in panel **(C)**. Aβ levels were increased in the HIP of PBS-injected mice exposed to CFC ENC and back to HC levels in the DAPT-injected group (condition effect [$F_{2,6} = 37.37, p < .001$]). All data are normalized to HC HIP samples, averaged per group and plotted as mean ± SEM; $n = 3/4$ mice per group. $***p < .001$ compared with HC control mice; $###p < .001$ for PBS-DAPT comparisons. **(E)** Native dot blot analysis by conformational OC antibody, recognizing fibrillar oligomers, in TBS-soluble HIP extracts from Tg2576 mice in the CFC ENC condition (injected with DAPT or PBS) or HC control mice. α-Tubulin was used as loading control. As the OC antibody is not Aβ sequence–specific, DAPT treatment results confirm the Aβ composition of OC-positive spots. **(F)** Quantification of OC/α-tubulin dot blot immunoreactivity ratio from groups in panel **(E)**. Levels of OC-reactive oligomers increased after CFC ENC in PBS-injected mice and back to HC levels with DAPT injection (condition effect [$F_{2,15} = 4.48, p < .05$]). Data are averaged per group and plotted as mean ± SEM; $n = 5/7$ mice per group. $*p < .05$ compared with HC; $#p < .05$ for differences between PBS- and DAPT-injected groups. **(G)** Immunostaining with OC antibody (red) revealed CFC-induced intracellular oligomeric deposits in CA1 neurons. DAPI (blue) counterstains cell bodies. **(H)** Native dot blot analysis by OC antibody in TBS with 1% Triton X-100 HIP extracts from Tg2576 mice in the CFC ENC or HC conditions. α-Tubulin was used as loading control. **(I)** Quantification of OC/α-tubulin immunoreactivity ratio from groups in panel **(H)** confirmed the intracellular localization of Aβ fibrillar oligomers (condition effect [$F_{1,11} = 9.19, p < .05$]). Data are averaged per group and plotted as mean ± SEM; $n = 6/7$ mice per group. $*p < .05$.

by native dot blot analysis in TBS extracts. OC immunoreactivity (Figure 4E, F), but not A11 immunoreactivity (Supplemental Figure S5E), was significantly enhanced in mice after CFC encoding in the PBS-injected group ($p < .05$) and was reduced to HC control levels in the DAPT-injected group ($p > .05$).

Interestingly, by immunofluorescence we observed a prevailing intracellular OC labeling in the cell layer and the stratum radiatum of hippocampal slices of CFC-trained mice (Figure 4G). The intracellular localization of OC-positive Aβ oligomers was confirmed by dot blot analysis on TBS with 1% Triton X-100 hippocampal extracts (Figure 4H, I), whose immunoreactivity quantification was consistent with the trend of TBS soluble extracts reported above.

Overall, we demonstrated that CFC encoding induces a strong Aβ oligomerization along selective pathways of OC-positive fibrillar oligomers, which are mainly detected inside neurons. DAPT treatment is effective in reducing levels of 14-kDa and OC-positive Aβ oligomers, suggesting that the largest amount of oligomerization occurs on de novo produced Aβ.

Blocking Aβ Production in the Hippocampus of Tg2576 Mice Restores Spine Rearrangements in Both the CA1 Subregion and BLA

As Aβ has been reported to block the growth of new synapses (24), we asked whether CFC-related Aβ release in the hippocampus has a causal role in the lack of synaptic rearrangements in this region. To test this possibility, we measured spine density in DAPT-injected Tg2576 mice sacrificed after CFC recall. Of note, DAPT has no impact on CFC memory, as
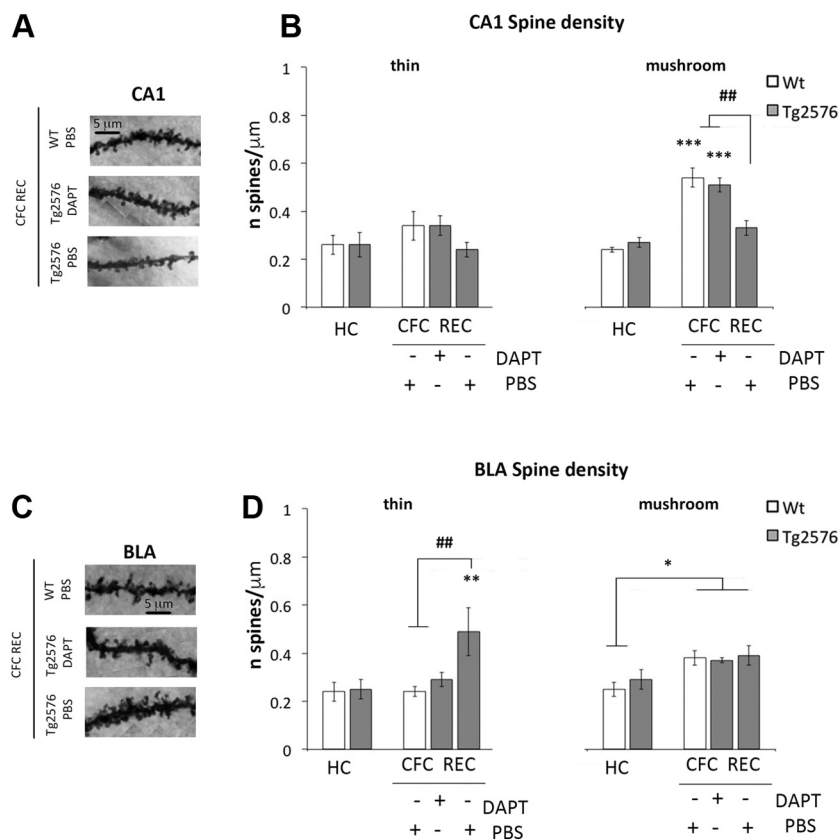
Figure 5. Intrahippocampal DAPT injection restores normal patterns of dendritic spines rearrangements in both the CA1 subregion and basolateral amygdala (BLA). Tg2576 mice received intrahippocampal injection of DAPT or phosphate-buffered saline (PBS) vehicle 15 hours before contextual fear conditioning (CFC) encoding. As a control condition for the effect of injections on spines, wild-type (Wt) mice were injected with PBS at the same time point. Twenty-four hours after injections, mice were subjected to CFC recall (REC) and sacrificed after a further 24 hours for spine counting. Home cage (HC) control mice were sacrificed in parallel. **(A)** z-Stack projections of dendritic segments from coronal sections containing the hippocampal CA1 subregion. Images are representative for DAPT- or PBS-injected Tg2576 mice and PBS-injected Wt mice sacrificed after CFC REC. **(B)** Spine density (n spines/μm) measured on thin and mushroom spines along CA1 apical dendrites in mice from groups as in panel **(A)**. See also Supplemental Figure S9 for filopodia and chubby/stubby spines. CFC was associated with a significant increase of mushroom spines as compared with HC control mice in the group of Tg2576 mice that received DAPT injection and in Wt mice with PBS injection, but not in Tg2576 mice that received PBS injection ($F_{4,30} =$ 7.39; $p < .001$). No differences among groups were reported for thin spines ($F_{4,30} = 2.49$, $p > .05$). $n = 2/3$ neurons per mouse, 3 mice per group. ***$p < .001$ as compared with HC control mice; ##$p < .01$ as compared with both Wt mice and DAPT-injected Tg2576 mice. **(C)** z-Stack projections of dendritic segments from coronal sections containing the BLA. Groups as in panel **(A)**. **(D)** Spine density (n spines/μm) measured on thin and mushroom spines along BLA dendrites in mice from groups in panel **(C)**. See also Supplemental Figure S9 for filopodia and chubby/stubby spines. Upon CFC REC, the number of thin spines was significantly increased from HC in PBS-injected Tg2576 mice, but was restored to Wt levels in DAPT-injected Tg2576 mice (condition effect [$F_{4,49} = 4.58$, $p < .01$]). As compared with relative HC control mice, the number of mushroom spines was significantly increased after CFC in all groups of CFC-trained mice ($F_{4,49} = 3.32$, $p < .05$). $n = 3/4$ neurons per mouse, 3 mice per group. *$p < .05$ and **$p < .01$ compared with HC control mice, ##$p < .01$ as compared with both Wt mice and DAPT-injected Tg2576 mice.

freezing behavior was unvaried in Tg2576 mice upon DAPT injection (Supplemental Figure S9).

We reported that the relative proportion of the four spine categories along CA1 apical dendrites were comparable between WT mice and Tg2576 mice that received intrahippocampal injection of DAPT (Figure 5A, B; Supplemental Figure S9). In detail, the CFC-induced increase of mushroom spines was evident in both DAPT-injected Tg2576 and control PBS-injected WT mice ($p < .001$ for both as compared with relative HC control mice) but not PBS-injected Tg2576 mice (Figure 5A, B). No differences were detected between groups for the other three spine categories (Figure 5B; Supplemental Figure S9). These data support the possibility that reducing Aβ restores the CFC-induced formation and maturation of spines in the hippocampus of Tg2576 mice.

We next formulated the corollary hypothesis that spine rearrangements in the BLA of Tg2576 mice compensate for the lack of spine formation in the hippocampus. To test this hypothesis, we measured CFC-induced spine changes in the BLA of mice that received intrahippocampal injection of DAPT. On BLA dendrites of Tg2576 mice exposed to CFC (Figure 5D), we found that the number of thin spines was restored to control WT levels in the DAPT group ($p > .05$), while it remained elevated in the PBS group ($p < .01$ as compared with

HC control mice). Rather, we found that the number of CFC-induced mushroom spines was comparable between Tg2576 and WT mice ($p > .05$), confirming the lack of a genotype effect on this spine category; also, the density of mushroom spines was unaffected by DAPT injection ($p > .05$) in Tg2576 mice. The relative proportions of filopodia and chubby spines were unaffected by DAPT (Supplemental Figure S9). Overall, the above data indicate that blocking Aβ accumulation in the hippocampus rescues synaptic changes associated with memory formation in this region and also reduces compensatory rearrangements taking place in the amygdala.

DISCUSSION

We demonstrate that within 24 hours from CFC exposure, Aβ oligomers accumulate in the hippocampus, but not in the amygdala, of asymptomatic Tg2576 mice. As a consequence of this activity-dependent Aβ rise, c-Fos activation measured in Tg2576 mice upon CFC memory recall is basically absent in the CA1 region of the hippocampus, and stronger in the BLA as compared with nonmutant mice. In line with this pattern of activation, Tg2576 mice do not form dendritic spines in the CA1 subfield of the hippocampus, while a considerable increase of spines is reported in the BLA after CFC. Altogether,

these data suggest that the two regions are in a homeostatic balance and can be differentially activated by presymptomatic AD mice to accomplish a memory task.

Our data are in line with functional magnetic resonance imaging studies reporting over- or underactivation of specific brain regions in individuals positive for amyloid load (4,37), but one question emerging is why the amygdala, but not other brain regions connected to the CA1 subregion, compensates for the hippocampal dysfunction. One possible explanation comes from the evidence that the BLA, but not the other regions, has been reported to coactivate with the CA1 subregion during the recall of fear memory (31), suggesting that the hippocampus and amygdala belong to a common network engaged during the formation of fear memories.

In light of literature showing that the amygdala accounts for the emotional tagging of memories (19), while the hippocampus integrates multiple information that converges into a memory trace (18), our results suggest that a shift in regional brain activation implicates a parallel change of the cognitive strategy, with a prevalence of emotional processing in AD mice. Of note, a similar cognitive shift in humans, a process referred to as cognitive reserve, has been reported during aging and early AD stages, and it is associated with the recruitment of neuronal networks alternative to canonical ones (38,39). In this framework, our study provides the first evidence that cognitive reserve is also supported by rearrangements of synaptic circuits underlying memory.

Of relevance, we provide the novel evidence that OC-positive fibrillar $A\beta$ oligomers, previously classified as type 2 and known to be confined to the vicinity of $A\beta$ plaques in aged Tg2576 mice (40), can be formed in the same mouse model at presymptomatic stages by exposition to CFC. We provide sequential proofs that link local vulnerability to $A\beta$ oligomerization with both the lack of synaptic rearrangements in the CA1 subregion and the compensatory synaptic changes in the BLA: 1) $A\beta$ oligomers accumulate in the hippocampus, but not in the amygdala, upon neuronal activation associated with the encoding of CFC memory; 2) CFC-induced $A\beta$ oligomers block synapse formation in the hippocampus; and 3) pharmacological prevention of $A\beta$ production in the hippocampus restores CFC-induced spine rearrangements to WT levels not only in this region, but also in the BLA.

As $A\beta$ production and oligomerization are activity dependent, the selective vulnerability of the hippocampus to $A\beta$ oligomers is intriguing. Within 24 hours of CFC encoding, $A\beta$ accumulates and oligomerizes in the hippocampus, but not in the amygdala. We can speculate that this depends on regional differences in $A\beta$ metabolism (i.e., production, oligomerization, and clearance) or intrinsic properties of the two tissues (prevalence of excitatory vs. inhibitory neurons). For example, gamma oscillations, which favor microglia-mediated $A\beta$ elimination and are frequent in the amygdala (41), are reduced in the hippocampus of AD 5xFAD mice (42).

While we previously reported (28) that dendritic spines in the hippocampus are intact in 2-month-old Tg2576 mice under HC conditions, here we show that in Tg2576 mice at this age, CFC triggers (through $A\beta$) spine alterations that are absent in baseline conditions. This suggests that cognitive stimulation that directly impacts on hippocampal activity is detrimental, with relevant implications for the translational aspects of our

findings. Our data are in apparent contradiction to reports of beneficial effects of enriched environmental stimulation in AD mice (43–45) and human studies indicating that active lifestyle protects against dementia (46–48). However, it is also known that exposing AD patients to intense intellectual demand can, rather, enhance $A\beta$ load and hasten AD progression (49,50). Together, these findings suggest that general stimulation is beneficial for individuals at risk for AD, while intense activity that impacts regions supporting high cognitive functions can be deleterious. We hypothesized the existence of a threshold of cognitive activity or stress, above which neuronal stimulation damages AD brains. Supporting this possibility, we here report that an increase of $A\beta$ is also found in mice exposed to the MWM, although to a lesser extent as compared with CFC. Indeed, the MWM is a memory task that, like CFC, is hippocampal dependent but requires the implementation of an active and likely less stressful motor response as compared with the memorization of a traumatic event. Consistent with our hypothesis, clinical studies demonstrate that stress disorders increase the risk of dementia (51,52), and clinicians commonly report that stressful events can trigger AD symptoms in aged individuals.

Concerning the translational potential of our findings, we suggest that the concomitant presence of $A\beta$ and atypical neuronal activation, both of which are detectable with PET scans (53), can represent the starting point for preclinical intervention in humans. In these terms, our study further supports the emerging idea that pharmacological interventions aimed not only at reducing $A\beta$, but also at contrasting its oligomerization or neutralizing $A\beta$ toxic oligomeric species (54,55), should start at preclinical AD stages to contrast $A\beta$ accumulation at its onset.

ARTICLE INFORMATION

From the Laboratory of Psychobiology (AP, GC, MA-T), Department of Experimental Neurology, Santa Lucia Foundation; Institute of Cell Biology and Neurobiology (AP, MA-T, SM), National Research Council; and European Brain Research Institute-Fondazione Rita Levi Montalcini (GM), Rome, Italy; Department of Molecular and Cellular Neurobiology Laboratory of Molecular Basis of Behavior (RP), Nencki Institute of Experimental Biology, Polish Academy of Sciences, Warsaw, Poland; Department of Pharmacology & Toxicology and Center for Chemistry and Biomedicine (VF), University of Innsbruck, Innsbruck, Austria; and the Department of Experimental Biomedical Sciences (RB), Lund University, Lund, Sweden.

Address correspondence to Silvia Middei, Ph.D., IBCN-CNR, Via del Fosso di Fiorano 64, 00143 Rome, Italy; E-mail: silvia.middei@cnr.it; or Giovanni Meli, Ph.D., EBRI, Viale Regina Elena 295, 00161 Rome, Italy; E-mail: g.meli@ebri.it.

REFERENCES

1. Bennett DA, Schneider JA, Arvanitakis Z, Kelly JF, Aggarwal NT, Shah RC, Wilson RS (2006): Neuropathology of older persons without cognitive impairment from two community-based studies. Neurology 66:1837–18144.
2. Aizenstein HJ, Nebes RD, Saxton JA, Price JC, Mathis CA, Tsopelas ND, et al. (2008): Frequent amyloid deposition without significant cognitive impairment among the elderly. Arch Neurol 65:1509–1517.
3. Morris JC, Roe CM, Xiong C, Fagan AM, Goate AM, Holtzman DM, Mintun MA (2010): APOE predicts amyloid-beta but not tau Alzheimer pathology in cognitively normal aging. Ann Neurol 67:122–131.
4. Sperling R (2011): Potential of functional MRI as a biomarker in early Alzheimer's disease. Neurobiol Aging 32(suppl 1):S37–S43.
5. Bateman RJ, Xiong C, Benzinger TL, Fagan AM, Goate A, Fox NC, et al. (2012): Dominantly inherited Alzheimer network. Clinical and biomarker changes in dominantly inherited Alzheimer's disease. N Engl J Med 30(367):795–804.
6. Fleisher AS, Chen K, Quiroz YT, Jakimovich LJ, Gomez MG, Langois CM, et al. (2012): Florbetapir PET analysis of amyloid-β deposition in the presenilin 1 E280A autosomal dominant Alzheimer's disease kindred: A cross-sectional study. Lancet Neurol 11:1057–1065.
7. Villemagne VL, Burnham S, Bourgeat P, Brown B, Ellis KA, Salvado O, et al. (2013): Amyloid β deposition, neurodegeneration, and cognitive decline in sporadic Alzheimer's disease: A prospective cohort study. Lancet Neurol 12:357–367.
8. Filippini N, MacIntosh BJ, Hough MG, Goodwin GM, Frisoni GB, Smith SM, et al. (2009): Distinct patterns of brain activity in young carriers of the APOE-epsilon4 allele. Proc Natl Acad Sci U S A 28(106):7209–7214.
9. Elman JA, Oh H, Madison CM, Baker SL, Vogel JW, Marks SM, et al. (2014): Neural compensation in older people with brain amyloid-β deposition. Nat Neurosci 17:1316–1318.
10. Stern Y (2009): Cognitive reserve. Neuropsychologia 47:2015–2028.
11. Barulli D, Stern Y (2013): Efficiency, capacity, compensation, maintenance, plasticity: emerging concepts in cognitive reserve. Trends Cogn Sci 17:502–509.
12. Mondadori CR, Buchmann A, Mustovic H, Schmidt CF, Boesiger P, Nitsch RM, et al. (2006): Enhanced brain activity may precede the diagnosis of Alzheimer's disease by 30 years. Brain 129:2908–2922.
13. Terry D, Sabatinelli D, Puente AN, Lazar NA, Miller LS (2015): A meta-analysis of fMRI activation differences during episodic memory in Alzheimer's disease and mild cognitive impairment. J Neuroimaging 25:849–860.
14. Palop JJ, Mucke L (2010): Amyloid-beta-induced neuronal dysfunction in Alzheimer's disease: From synapses toward neural networks. Nat Neurosci 13:812–818.
15. Restivo L, Vetere G, Bontempi B, Ammassari-Teule M (2009): The formation of recent and remote memory is associated with time-dependent formation of dendritic spines in the hippocampus and anterior cingulate cortex. J Neurosci 29:8206–8214.
16. Middei S, Houeland G, Cavallucci V, Ammassari-Teule M, D'Amelio M, Marie H (2013): CREB is necessary for synaptic maintenance and learning-induced changes of the AMPA receptor GluA1 subunit. Hippocampus 23:488–499.
17. Pignataro A, Middei S, Borreca A, Ammassari-Teule M (2013): Indistinguishable pattern of amygdala and hippocampus rewiring following tone or contextual fear conditioning in C57BL/6 mice. Front Behav Neurosci 7:156.
18. Maren S, Phan KL, Liberzon I (2013): The contextual brain: Implications for fear conditioning, extinction and psychopathology. Nat Rev Neurosci 14:417–428.
19. LeDoux JE (2000): Emotion circuits in the brain. Annu. Rev. Neurosci 23:155–184.
20. Lamprecht R, LeDoux J (2004): Structural plasticity and memory. Nat Rev Neurosci 5:45–54.
21. Bero AW, Yan P, Roh JH, Cirrito JR, Stewart FR, Raichle ME, et al. (2011): Neuronal activity regulates the regional vulnerability to amyloid-β deposition. Nat Neurosci 14:750–756.
22. Shankar GM, Li S, Mehta TH, Garcia-Munoz A, Shepardson NE, Smith I, et al. (2008): Amyloid-beta protein dimers isolated directly from Alzheimer's brains impair synaptic plasticity and memory. Nat Med 14:837–842.
23. Selkoe DJ, Hardy J (2016): The amyloid hypothesis of Alzheimer's disease at 25 years. EMBO Mol Med 8:595–608.
24. Zhao Y, Sivaji S, Chiang MC, Ali H, Zukowski M, Ali S, et al. (2017): Amyloid beta peptides block new synapse assembly by nogo receptor-mediated inhibition of T-type calcium channels. Neuron 11(96):355–372.e6.
25. Kamenetz F, Tomita T, Hsieh H, Seabrook G, Borchelt D, Iwatsubo T, et al. (2003): APP processing and synaptic function. Neuron 37:925–937.
26. Cirrito JR, Yamada KA, Finn MB, Sloviter RS, Bales KR, May PC, et al. (2005): Synaptic activity regulates interstitial fluid amyloid-beta levels in vivo. Neuron 48:913–922.
27. Hsiao K, Chapman P, Nilsen S, Eckman C, Harigaya Y, Younkin S, et al. (1996): Correlative memory deficits, Abeta elevation, and amyloid plaques in transgenic mice. Science 274:99–102.
28. D'Amelio M, Cavallucci V, Middei S, Marchetti C, Pacioni S, Ferri A, et al. (2011): Caspase-3 triggers early synaptic dysfunction in a mouse model of Alzheimer's disease. Nat Neurosci 14:69–76.
29. Meli G, Lecci A, Manca A, Krako N, Albertini V, Benussi L, et al. (2014): Conformational targeting of intracellular Aβ oligomers demonstrates theirpathological oligomerization inside the endoplasmic reticulum. Nat Commun 5:3867.
30. Bezzina C, Verret L, Juan C, Remaud J, Halley H, Rampon C, Dahan L (2015): Early onset of hypersynchronous network activity and expression of a marker of chronic seizures in the Tg2576 mouse model of Alzheimer's disease. PLoS One 10:e0119910.
31. Wheeler AL, Teixeira CM, Wang AH, Xiong X, Kovacevic N, Lerch JP, et al. (2013): Identification of a functional connectome for long-term fear memory in mice. PLoS Comput Biol 9:e1002853.
32. Portera-Cailliau C (2012): Which comes first in fragile X syndrome, dendritic spine dysgenesis or defects in circuit plasticity. Neuroscientist 18:28–44.
33. Oddi D, Subashi E, Middei S, Bellocchio L, Lemaire-Mayo V, Guzmán M, et al. (2015): Early social enrichment rescues adult behavioral and brain abnormalities in a mouse model of fragile X syndrome. Neuropsychopharmacology 40:1113–1122.
34. Béïque JC, Andrade R (2003): PSD-95 regulates synaptic transmission and plasticity in rat cerebral cortex. J Physiol 546:859–867.
35. Kayed R, Head E, Sarsozam F, Saingm T, Cotman CW, Necula M, et al. (2007): Fibril specific, conformation dependent antibodies recognize a generic epitope common to amyloid fibrils and fibrillar oligomers that is absent in prefibrillar oligomers. Mol Neurodegener 2:18.
36. Kayed R, Head E, Thompson JL, McIntire TM, Milton SC, Cotman CW, Glabe CG (2003): Common structure of soluble amyloid oligomers implies common mechanism of pathogenesis. Science 300:486–489.
37. Huijbers W, Mormino EC, Wigman SE, Ward AM, Vannini P, McLaren DG, et al. (2014): Amyloid deposition is linked to aberrant entorhinal activity among cognitively normal older adults. J Neurosci 34:5200–5210.
38. Stern Y, Moeller JR, Anderson KE, Luber B, Zubin NR, DiMauro AA, et al. (2000): Different brain networks mediate task performance in normal aging and AD: defining compensation. Neurology 55:1291–1297.
39. Dickerson BC, Salat DH, Greve DN, Chua EF, Rand-Giovannetti E, Rentz DM, et al. (2005): Increased hippocampal activation in mild cognitive impairment compared with normal aging and AD. Neurology 65:404–411.
40. Liu P, Reed MN, Kotilinek LA, Grant MK, Forster CL, Qiang W, et al. (2015): Quaternary structure defines a large class of amyloid-β oligomers neutralized by sequestration. Cell Rep 11:1760–1771.

41. Randall FE, Whittington MA, Cunningham MO (2011): Fast oscillatory activity induced by kainate receptor activation in the rat basolateral amygdala in vitro. Eur J Neurosci 33:914–922.

42. Iaccarino HF, Singer AC, Martorell AJ, Rudenko A, Gao F, Gillingham TZ, et al. (2016): Gamma frequency entrainment attenuates amyloid load and modifies microglia. Nature 540:230–235.

43. Maesako M, Uemura K, Kubota M, Kuzuya A, Sasaki K, Hayashida N, et al. (2012): Exercise is more effective than diet control in preventing high fat diet-induced β-amyloid deposition and memory deficit in amyloid precursor protein transgenic mice. J Biol Chem 287:23024–23033.

44. Verret L, Krezymon A, Halley H, Trouche S, Zerwas M, Lazouret M, et al. (2013): Transient enriched housing before amyloidosis onset sustains cognitive improvement in Tg2576 mice. Neurobiol Aging 34:211–225.

45. Rodríguez JJ, Noristani HN, Verkhratsky A (2015): Microglial response to Alzheimer's disease is differentially modulated by voluntary wheel running and enriched environments. Brain Struct Funct 220:941–953.

46. Verghese J, Lipton RB, Katz MJ, Hall CB, Derby CA, Kuslansky G, et al. (2003): Leisure activities and the risk of dementia in the elderly. N Engl J Med 348:2508–2516.

47. Andel R, Vigen C, Mack WJ, Clark LJ, Gatz M (2006): The effect of education and occupational complexity on rate of cognitive decline in Alzheimer's patients. J Int Neuropsychol Soc 12:147–152.

48. Mistridis P, Mata J, Neuner-Jehle S, Annoni JM, Biedermann A, Bopp-Kistler I, et al. (2017): Use it or lose it! Cognitive activity as a protective factor for cognitive decline associated with Alzheimer's disease. Swiss Med Wkly 147:w14407.

49. Buckner RL, Snyder AZ, Shannon BJ, LaRossa G, Sachs R, Fotenos AF, et al. (2005): Molecular, structural, and functional characterization of Alzheimer's disease: Evidence for a relationship between default activity, amyloid, and memory. J Neurosci 25:7709–7717.

50. Oh H, Razlighi QR, Stern Y (2018): Multiple pathways of reserve simultaneously present in cognitively normal older adults. Neurology 90:e197–e205.

51. Qureshi SU, Kimbrell T, Pyne JM, Magruder KM, Hudson TJ, Petersen NJ, et al. (2010): Greater prevalence and incidence of dementia in older veterans with posttraumatic stress disorder. J Am Geriatr Soc 58:1627–1633.

52. Yaffe K, Vittinghoff E, Lindquist K, Barnes D, Covinsky KE, Neylan T, et al. (2010): Posttraumatic stress disorder and risk of dementia among US veterans. Arch Gen Psychiatry 67:608–613.

53. Maya Y, Okumura Y, Kobayashi R, Onishi T, Shoyama Y, Barret O, et al. (2016): Preclinical properties and human in vivo assessment of 123I-ABC577 as a novel SPECT agent for imaging amyloid-β. Brain 139:193–203.

54. Sevigny J, Chiao P, Bussière T, Weinreb PH, Williams L, Maier M, et al. (2016): The antibody aducanumab reduces Aβ plaques in Alzheimer's disease. Nature 537:50–56.

55. Van Dyck CH (2018): Anti-amyloid-β monoclonal antibodies for Alzheimer's disease: Pitfalls and promise. Biol Psychiatry 83:311–319.